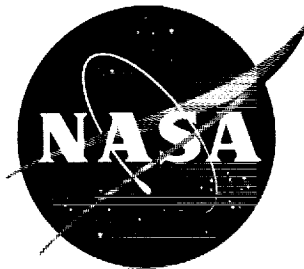


37p.

162-14323

NASA TN D-1379

RIGHT IN COPY



TECHNICAL NOTE

D-1379

STATIC LONGITUDINAL STABILITY AND PERFORMANCE OF
SEVERAL BALLISTIC SPACECRAFT CONFIGURATIONS

IN HELIUM AT A MACH NUMBER OF 24.5

By Patrick J. Johnston and Curtis D. Snyder

Langley Research Center
Langley Station, Hampton, Va.

**CASE FILE
COPY**

NATIONAL AERONAUTICS AND SPACE ADMINISTRATION
WASHINGTON

August 1962

100

100

100

100

100

100

100

100

NATIONAL AERONAUTICS AND SPACE ADMINISTRATION

TECHNICAL NOTE D-1379

STATIC LONGITUDINAL STABILITY AND PERFORMANCE OF
SEVERAL BALLISTIC SPACECRAFT CONFIGURATIONS
IN HELIUM AT A MACH NUMBER OF 24.5

By Patrick J. Johnston and Curtis D. Snyder

SUMMARY

The static longitudinal stability and performance characteristics of three similar spacecraft configurations were determined at a Mach number of 24.5 in helium. The angle-of-attack range covered in these tests was from -8° to 188° , and the Reynolds number, based on maximum configuration diameter, was 0.57×10^6 .

The results obtained on the three similar configurations were compared and, on the basis of developing the greatest lift-drag ratio without exposing the afterbody to the flow, the configuration incorporating a 35° half-angle conical afterbody and a heat-shield corner radius of 5 percent of the maximum diameter proved to be superior. Further, the results showed that this configuration required next to the minimum lateral center-of-gravity displacement for trimming at a given lift coefficient or lift-drag ratio.

A comparison of longitudinal data obtained in nitrogen and helium on the same blunt-nose spacecraft configuration at Mach numbers of 18 and 24.5, respectively, indicated that results obtained in helium on this specific shape had smaller normal-force- and pitching-moment-curve slopes and lower axial-force coefficients. Lift-drag ratios showed generally good agreement except near the maximum. The lift results obtained in the two gases showed excellent agreement up to the maximum.

Some additional tests were made to determine the effectiveness of a small chin flap mounted on a blunt-face spacecraft configuration. The flap, representing about 4.1 percent of the projected frontal area of the spacecraft configuration was most effective in the range of deflection angles less than about 100° .

INTRODUCTION

The advantages of a pure ballistic manned reentry system were first pointed out in reference 1. Operational reliability proved to be one of the most attractive features of the symmetrical spacecraft configuration. Later studies (refs. 2 and 3) indicated that even small amounts of lift can be highly advantageous from the viewpoint of atmospheric entry mechanics. It has been shown, for instance (ref. 4), that for a given peak deceleration, a small lift-drag ratio can have significant effects on the corridor widths available to vehicles reentering the atmosphere at velocities in excess of orbital speed.

One class of manned reentry vehicles under consideration for extra-terrestrial missions are those which combine the attractive features of a symmetrical, ballistic-type capsule along with some trim-control schemes such as aerodynamic flaps, reaction jets, vehicle center-of-gravity displacements, and/or combinations of these. Such a class of vehicles might be referred to as semiballistic spacecraft configurations since they offer advantages common to both symmetrical and lifting vehicles.

Because of the possibility of unusual attitudes or unforeseen disturbances during reentry as well as abort maneuvers, a need exists for experimental data at hypersonic Mach numbers throughout the entire angle-of-attack range of the vehicle.

The purpose of the present investigation was to determine experimentally and to compare the longitudinal static stability and performance characteristics of three similar blunt-face axisymmetric bodies throughout the complete angle-of-attack range. The configurations had common heat-shield face radii, projected frontal areas, and essentially equal volumes but differed in face corner radius and afterbody cone angle.

Some additional tests were made to determine the trim effectiveness of a small chin flap on a second ballistic-type configuration.

All the tests were conducted at a Mach number of approximately 24.5 in helium. The Reynolds number was about 0.57×10^6 , based on the maximum configuration diameter.

Helium has been used in wind tunnels in recent years for generating flow at high Mach numbers while avoiding the high temperatures and pressures associated with air operation at high hypersonic speeds. The resulting problems of transforming data obtained in helium to equivalent air data have therefore been of some concern (ref. 5). As more data become available for comparison purposes, simple parameters based on similarity rules have been found effective in correlating helium and air data for some relatively slender configurations (ref. 6). The full

extent to which model geometry, for instance, might affect such comparisons has yet to be fully determined. Despite the present uncertainties regarding the degree of air simulation which may be expected with helium, it is reasonable to assume that conclusions drawn from comparative stability and performance tests made in helium should still prove valid when applied to similar configurations in air. It is primarily with this viewpoint that the present results have been analyzed. In order to provide some additional information on the air-helium simulation problem and to indicate the usefulness of helium as a test medium, some results obtained in the present tests are compared with similar data obtained at a Mach number of 18 in nitrogen.

SYMBOLS

A sketch of a typical configuration showing positive directions of forces and moments is presented in figure 1.

A_f	flap area, sq in.
C_A	axial-force coefficient, $\frac{\text{Total axial force}}{qS}$
C_D	drag coefficient, $C_A \cos \alpha + C_N \sin \alpha$
C_L	lift coefficient, $C_N \cos \alpha - C_A \sin \alpha$
C_{L_α}	lift-curve slope per degree at $\alpha = 0^\circ$
L/D	lift-drag ratio
C_m	pitching-moment coefficient, $\frac{\text{Pitching moment}}{qSD}$
ΔC_m	incremental pitching-moment coefficient of flap
C_N	normal-force coefficient, $\frac{\text{Normal force}}{qS}$
C_p	pressure coefficient, $\frac{P - P_\infty}{q_\infty}$
D	maximum body diameter, in.
M	free-stream Mach number

p_t	stagnation pressure, lb/sq in.
p	static pressure, lb/sq in.
q	dynamic pressure, lb/sq in.
R	Reynolds number (based on maximum configuration diameter)
S	maximum projected frontal area, sq in.
α	angle of attack, deg
γ	ratio of specific heats
δ_f	flap deflection, deg
θ	afterbody cone semivertex angle, deg
x	distance along the body longitudinal axis, in.
y	vertical distance from body center line, in.

Subscripts:

max	maximum
∞	free stream
cg	center of gravity

APPARATUS

General Description of the Tunnel

The tests were conducted in the Langley 22-inch helium tunnel. Briefly, this is an intermittent, closed-cycle facility in which helium is expanded through a 5° half-angle conical nozzle to a test section approximately 22 inches in diameter. The flow is then decelerated by means of a two-dimensional variable area supersonic and subsonic diffuser before entering two interconnected 60-foot-diameter vacuum spheres. The helium contained in these spheres along with whatever contaminating gases (principally air) which may have leaked into the low-pressure region of the system is recompressed to 5,000 pounds per square inch. The mixture is then purified by passing it through a liquid nitrogen refrigeration system and silica gel dryer thereby reducing the contaminati

agents to less than 0.02 percent by volume. Following the purification process, the helium is returned to the reservoir for reuse in subsequent tests. A sketch showing the principal dimensions of the nozzle and test section is shown in figure 2.

FLOW CALIBRATION

Local Mach numbers in the testing region were determined by a rather extensive pitot pressure survey, the principal results of which are shown in figure 3 as the average tunnel cross-section Mach number as a function of tunnel station (measured from the test-section window center line).

Pitot pressure ratios from which the average Mach numbers were determined were corrected for real-gas effects according to the method presented in reference 7.

The calibration results shown in figure 3 are characteristic of all flow distributions generated by conical nozzles in that a longitudinal Mach number gradient exists in the flow. For the present nozzle this gradient was small, having a value of about 0.08 per inch over the length of the calibrated region.

In addition to the longitudinal Mach number gradient, a second inherent feature of the flows produced by conical nozzles is that of flow divergence. The distribution of flow angularity caused by this divergence was not determined in the present calibration; however, it is not expected to seriously affect the results of the present tests for reasons which will be discussed subsequently.

Models

Details and dimensions of the models used in the present tests are shown in figures 4 to 6. As shown in figure 4, three similar configurations were tested having a common maximum body diameter and nose radius of 2.00 and 2.40 inches, respectively. The afterbody cone apexes were replaced with spherical segments having a common radius of 0.218 inch. Moment reference centers of the three configurations shown in figure 4 were located 0.576 inch rearward of the nose. The models were constructed of aluminum and the exterior surfaces were polished.

In order to obtain data over an angle-of-attack range from -8° to 188° , it was necessary to construct three models of each configuration shown in figure 4. The alterations required, method of mounting, and angle-of-attack range covered by each of these models are illustrated in figure 5.

Some additional tests were made to determine the effectiveness of a small chin flap on a blunt-face axisymmetric body; for these tests an existing model was used with the flap attached as shown in figure 6. The effective area of this flap constituted about 4.1 percent of the projected frontal area of the basic model.

TESTS AND ACCURACY

All tests were conducted at a stagnation pressure automatically regulated at 1,000 lb/sq in. gage. Stagnation temperatures diminished about 20° F during the course of each test as a result of the decreasing reservoir pressure; an average of 60° F was chosen to be representative. The Mach number at the nose of the models was 24.5 except for the tests to determine flap effectiveness. This model was mounted on a second two-component strain-gage balance slightly longer than the original; consequently, the model was located farther upstream and the corresponding nose Mach number was 24.3. The Reynolds number based on the above conditions and the model diameter was 0.57×10^6 .

Although flow angularity and Mach number gradients exist in the test region, their effects on the model force and moment measurements were minimized by maintaining the axis of model rotation on the tunnel center line. Furthermore, the relatively small model size (compared to the tunnel dimensions) also tended to minimize the effects flow angularity and gradients might have on the data.

During a particular test the hydraulically actuated sting mechanism supporting the model-balance assembly was continuously traversed through a maximum range of $\pm 20^\circ$ at a rate generally not exceeding 3° per second. An optical system was used to obtain data at specific angles of attack. Briefly, in this system a lens-prism assembly was mounted on the model and reflected light from a point source onto a steel plate adjacent to the test section. Small photoelectric cells were magnetically attached to the steel plate at calibrated intervals. As the reflected light swept past each photoelectric cell, an electrical relay was energized causing a high-speed digital recorder to sample and record the strain-gage-balance outputs on magnetic tape.

As a consequence of the physical size of the photoelectric cells, small differences were expected in the data (at a given angle of attack) depending on the direction from which the reflected light approached the cells. Since the photoelectric cells were approached from both directions during the course of a test, two sets of data were obtained at each angle of attack and, when feasible, both are presented to indicate the magnitudes of these differences. (See fig. 7, for example.)

The differences varied from test to test and were primarily due to the physical arrangement of the optical system and the size of the photo-electric cells. The scatter shown in figure 7 also serves to indicate the overall accuracy of this method of obtaining force and moment data including the accuracy of the three-component strain-gage balance.

Model base pressures were not measured during the tests because the models were continuously rotating in pitch. In view of the relative magnitudes of forebody drag and base pressure drag it was not believed worthwhile to make separate tests to determine base pressures for the purpose of adjusting the axial forces to a condition where free-stream pressures are acting on the model base.

RESULTS AND DISCUSSION

Longitudinal Performance of Three Similar Configurations

The basic results presented in figure 7 have been referred to the wind axis system and the longitudinal performance of the three vehicles is compared in figures 8 to 10; for clarity, only faired curves are shown in the latter figures.

The lift results obtained on the three configurations are compared in figure 8 and indicate that, in addition to developing the greatest lift, configuration 1 also has the largest initial lift-curve slope of the three configurations. The negative initial lift-curve slopes shown in figure 8 are a consequence of the high axial-force contribution of the blunt-face shapes to the lift component.

When the conical afterbodies of the vehicles are facing upstream, at angles of attack near 180° , the configurations have positive lift-curve slopes with maximum lifts occurring near $\alpha = 160^\circ$.

The effects of angle of attack on the drag coefficients of the three configurations are shown in figure 9. Maximum drag coefficients occur, of course, at zero angle of attack when the blunt heat shields are normal to the flow. The differences in configuration drag coefficients at zero angle of attack shown in the figure are essentially due to varying the heat-shield corner radii, neglecting incremental differences in drag due to the changes in afterbody geometry. Minimum drag coefficients of about 0.4 are observed to occur near an angle of attack of 70° for all three shapes.

Variations in afterbody cone angles as well as heat-shield corner radii contributed to the rather large differences in configuration drag coefficients at an angle of attack of 180° .

A comparison of the lift-drag ratios obtained on the three configurations over the angle-of-attack range is presented in figure 10. As shown in this figure, configuration 1 develops a substantially higher $(L/D)_{\max}$ than either configuration 2 or 3. It is significant to note in the data shown in figure 10 that the maximum lift-drag ratios of the three configurations are attained at angles of attack which would expose the afterbodies to the flow; consequently, a substantial weight penalty might be incurred in providing adequate afterbody heat protection in order to allow the vehicles to develop their full performance potential.

The following table summarizes the more important performance parameters for the three configurations:

Configuration	θ , deg	$C_{L\alpha}$	$C_{L,\max}$	$(L/D)_{\max}$	C_L at $\alpha = \theta$	L/D at $\alpha = \theta$
1	30	-0.23	-0.53	-0.72	-0.51	-0.48
2	35	-.22	-.49	-.67	-.49	-.53
3	40	-.19	-.43	-.59	-.43	-.52

By virtue of the fact that it has the highest lift-curve slope, maximum lift and maximum lift-drag ratio, configuration 1 is, from a performance viewpoint, clearly superior to the other two configurations tested. As is frequently the case, however, numerous other factors must be taken into consideration before a final choice can be made as to the best vehicle shape. Certainly, one of the most important factors which must be considered is aerodynamic heating; it is the intent in the following discussion to show how approaches to the solution of the heating problem can compromise the selection of configuration 1 on the basis of performance.

Although configuration 1 clearly has the best performance, the fact that it must operate at rather high angles of attack ($(L/D)_{\max}$, for example, occurs at $\alpha = 50^\circ$) in order to achieve its ultimate performance capability means that the edge of the heat shield will become, in fact, a leading edge. Since this configuration incorporates a sharp-edge heat shield, severe local aerodynamic heating in the vicinity of the sharp edge is to be anticipated when it is operated at angles of attack required to attain $C_{L,\max}$ and $(L/D)_{\max}$, for instance. It follows, therefore, that the severity of this local heating problem would likely lead to the alternative selection of one of the remaining shapes as the best compromise from a performance viewpoint.

An additional factor to be considered in the selection of capsule shape is that the angle-of-attack range available for operating these

vehicles might be limited by afterbody heating. One of the fundamental advantages of the capsule-type reentry vehicle is that the brunt of the intense aerodynamic heating is borne by the face; consequently the heat protection material is concentrated over that portion of the body. The afterbody, on the other hand, can remain relatively unprotected as long as it stays in the "shadowed" portion of the flow field. Following this design principle, the usable angle-of-attack range available for each of the configurations can be considered to be limited to angles for which the afterbodies are hidden behind the heat shield or at most become parallel to the free-stream velocity vector. The preceding table indicates that, although configuration 1 develops a slightly higher lift when $\alpha = 0$, configuration 2 attains a significantly higher lift-drag ratio when the angle of attack is limited to a value not exceeding the afterbody half-cone angle. Configuration 2, moreover, incorporates an edge radius on the heat shield which affords some mitigation of the local heating problem which would exist on a sharp-edge configuration.

Finally, it is to be noted in the table that configuration 2 is capable of exceeding $L/D = 1/2$ when $\alpha = 0$, a value which is generally conceded to be adequate from the viewpoint of guidance requirements, human tolerance to deceleration, and range control during reentry at superorbital speeds. An example of the extent to which L/D can influence the available reentry corridor of a vehicle returning at parabolic speed was shown in reference 4 where, under the restraint of a maximum deceleration limit of $10g$, an L/D capability of $1/2$ is sufficient to increase the corridor depth to about 32 international nautical miles in contrast to only about 6 miles for the ballistic case.

Configuration Stability

Figure 11 shows the variation of the experimental pitching-moment coefficients over the entire angle-of-attack range for the three configurations. The results presented in this figure indicate that the vehicles are statically stable about the moment reference center chosen for these tests up to an angle of attack near 40° . Over the complete angle-of-attack range three trim points occur, two of which are stable.

Of particular significance in the data of figure 11 is the fact that all three configurations are stable at an angle of attack of 180° . The significance lies in the fact that if these configurations are mounted on the launch vehicle as suggested in reference 1 - that is, with the heat shield rearward - the vehicles would be at a stable, trimmed attitude prior to some contingent abort maneuver. For a center of gravity located 0.288 diameter behind the heat-shield face, the vehicles would remain trimmed with the relatively unprotected afterbody exposed to high

aerodynamic-heating rates unless acted upon by some moment of sufficient magnitude to reorient the vehicle enabling the heat protection system to function properly. The required moment could be supplied by attitude control reaction jets or aerodynamic flaps; however, the launch weight penalty in extra fuel load for the reaction jets (over and above that required for orientation outside the atmosphere) or heat protection material for the flap might prove to be exorbitant. The simpler more reliable reorientation system is to allow aerodynamic forces to rotate the spacecraft configuration to the proper attitude; to this end, the data of figure 11 have been examined to determine the most rearward center-of-gravity position for each configuration which could permit only a single, stable trimmed attitude over the entire angle-of-attack range. The results of such an examination indicated that the vehicle centers of gravity would have to be located at 0.190, 0.148, and 0.128 diameter rearward of the heat-shield face for configurations 1 to 3, respectively, in order to establish a unique stable trim angle of attack at 0° . It might be found difficult, if not impossible, to stow internal equipment in a manner that would allow the center of gravity of configuration 3, for instance, to be located as close to the heat shield as 0.128 diameter.

Controls

There are several methods by which a reentry vehicle can be controlled during the atmospheric portion of the flight. For axisymmetric blunt-face vehicles, two methods which appear promising are the aerodynamic flap and a scheme utilizing a combination of an offset center of gravity and reaction jets. It is this latter technique which will be considered first.

Translation of the vehicle center of gravity small distances from the vehicle axis of symmetry can provide a symmetrical blunt-face configuration with considerable maneuver and range control during atmospheric reentry. In this scheme, lateral range variation can be accomplished by utilizing reaction jets for roll control. Since it is likely that a reaction jet attitude control system will be incorporated in the vehicle for orientation outside the atmosphere, the system could serve a dual purpose by permitting lateral range control after reentry has taken place.

Based upon these considerations, figure 12 has been prepared to show the extent of center-of-gravity displacement required to trim the three configurations at lift coefficients up to the maximum and lift-drag ratios up to the maximum. As indicated in figure 12, configuration 3 requires a considerably greater center-of-gravity displacement for trimming at a given C_L or L/D than either configurations 1 or 2, particularly at the higher lift coefficients.

On the basis of the results presented in figure 12, that is, requiring the minimum center-of-gravity displacement for trim at a given lift coefficient or lift-drag ratio, configuration 1 appears superior. As discussed previously, however, of the three configurations tested, the first has a lift-drag ratio capability about 10 percent below that of configurations 2 and 3 before exposing the afterbody to the flow. On the basis of having the highest L/D capability without exposing the afterbody to the flow and requiring next to the smallest center-of-gravity displacement for trimming at a given C_L or L/D , configuration 2 appears to have the superior geometry of the three configurations tested.

Another method of controlling a reentry configuration in the atmosphere is by the use of some type of aerodynamic flap. An earlier experimental investigation at $M = 9.6$ (ref. 8) indicated that one of the most effective types of control surface for a blunt-face vehicle is the chin flap. Since this type of control is directly exposed to the flow, it has greater effectiveness than an afterbody flap which, over a considerable range of angles of attack and deflection angles, would remain in that portion of the flow field having comparatively low dynamic pressures. Adequate protection for widely varying local heating rates over the flap and adjacent vehicle surfaces is probably one of the most critical problems to be overcome before the chin flap gains extensive use.

Some results of a test at $M = 24.3$ are presented in figure 13 to show the effects of deflecting a chin flap on the normal-force and pitching-moment characteristics of the blunt-face reentry configuration shown in figure 6. The effectiveness of this type of control surface was determined by measuring the incremental pitching moments due to flap deflection at angles of attack of 0° , 10° , and 20° and the results are presented in figure 14. The results of figure 14 at zero angle of attack indicate the flap to be most effective in the range of deflections between 45° and 100° . At the higher deflections the effectiveness is observed to be substantially diminished. At angles of attack greater than zero, the flap is more effective at small deflections since the angle between the free stream and the flap is increased correspondingly. The rapid loss in effectiveness at flap deflection angles beyond 120° is probably associated with flow separation over the flap and portions of the heat-shield face adjacent to the flap. It should be noted therefore, that variations in flap size or aspect ratio might considerably alter the flap effectiveness shown in the figure, particularly for deflection angles beyond 90° .

Air-Helium Simulation for Blunt Configurations

It is of interest, whenever possible, to compare data obtained in helium with corresponding air data to afford some basis for judging the qualitative value of data obtained by using helium as a test medium and

hence the degree of simulation to be expected from such tests. Many of the theoretical aspects of the air-helium simulation problems have been examined, as in reference 5, for example, but the full extent of the problem can only be determined by tests of the same configurations in both gases under identical flow conditions. Frequently, however, it is difficult to precisely duplicate such fundamentally important flow parameters as Mach number and Reynolds number. A comparison of the longitudinal force and moment results on several rather slender-wing configurations was made in reference 6 wherein it was shown that a correlation between air and helium data is possible based on flat-plate hypersonic similarity parameters. Additional correlations of force and moment results obtained in air and helium for a variety of wings, cones, slender, and blunt bodies have been summarized in reference 9 along with some preliminary results of the present investigation.

In order to permit a detailed assessment of the extent of air simulation which may be anticipated from tests of extremely blunt capsule-type configurations in helium, the longitudinal stability and performance results obtained on configuration 2 are presented in figures 15 and 16 along with similar unpublished experimental data obtained at an average Mach number of 18 and Reynolds number of 0.06×10^6 in a Hotshot tunnel at the Chance Vought Corporation. Nitrogen is used in this facility instead of air in order to reduce the chemical reactions of the gas in the nozzle. (Nitrogen and air, of course, have equivalent specific-heat ratios at standard conditions.) Since the chief source of the simulation problem arises as a result of difference in specific-heat ratios of air and helium ($7/5$ and $5/3$, respectively) any effects in the overall forces and moments due to changing γ should be evident in figures 15 and 16.

Although the comparison of experimental data shown in figures 15 and 16 is not ideal in view of the differences in Mach and Reynolds numbers, it is reasonable to assume the effects of the Mach number difference are of secondary importance. The order of magnitude difference in test Reynolds number, on the other hand, may have significant effects on drag and lift-drag ratio, for instance, and might obscure differences due to changing the specific-heat ratio.

In addition to comparing experimental data, figures 15 and 16 also include the results of some impact theory calculations obtained from the NASA Manned Spacecraft Center. The Newtonian results were modified by employing a stagnation pressure coefficient of 1.838 ($M = 18$, $\gamma = 7/5$) and 1.762 ($M = 24.5$, $\gamma = 5/3$) and, thus, can be considered air-modified and helium-modified Newtonian results. The configuration on which the theoretical results were obtained was identical to configuration 2 of the present tests except that the afterbody cone extremity was not rounded but extended to the apex. This discrepancy will not,

of course, affect the comparison at angles of attack below 35° because of afterbody shielding. At higher angles of attack, however, the effect this geometry difference will have on the comparisons is likely to become appreciable.

An examination of the configuration performance (fig. 15(a)) indicates that, except for the drag at small angles of attack, modified Newtonian theory is in excellent agreement with the test results obtained in helium. In particular, the predicted initial lift-curve slope, maximum lift, and maximum lift-drag ratio are observed to be in good agreement with the experimental data. Additionally, it is to be noted that although the experimental results obtained in nitrogen generally agree with the data obtained in helium, in some instances the nitrogen data fail to follow the trends indicated by employing the pitot pressure coefficient of modified impact theory. For example, although the lift results obtained in nitrogen and helium are in exceptionally close agreement, it would be anticipated from consideration of modified impact theory that the maximum lift measured in nitrogen would be slightly larger than that measured in helium.

The theoretical overprediction of drag near zero angle of attack is attributable to pressure relieving effects near the shoulder of the heat-shield face and has been observed in numerous earlier investigations.

The lift-drag ratios measured in nitrogen are observed to be lower than those measured in helium or predicted by modified Newtonian theory particularly near $(L/D)_{\max}$; these differences may be a consequence of the substantially lower Reynolds number of the nitrogen tests.

The variation with angle of attack of pitching-moment, axial-force, and normal-force coefficients predicted by modified impact theory and measured experimentally is presented in figure 15(b).

The measured pitching-moment results are observed to be quite similar and, in addition, follow the trends predicted by Newtonian theory modified by the employment of the stagnation pressure coefficient. The angle of attack for neutral stability, for instance, is observed to be identical for both experiments as well as theory.

Measurements of normal force in nitrogen were considerably higher than those obtained in helium and, moreover, substantially exceed the values predicted by theory.

The differences in experimentally determined normal-force and pitching-moment coefficients shown in figure 15(b) warrant an additional examination of the configuration stability. For this purpose the pitching moments of configuration 2 are shown in figure 16 as a function of

normal-force coefficient. The slopes of these data taken at $C_N = 0$ indicate the zero lift centers of pressure to be 0.738 diameter from the nose for the data obtained in nitrogen, 0.988 diameter for the helium tests, and 0.818 diameter as determined from impact theory. These substantial differences in center-of-pressure location diminish considerably at the higher angles of attack, however. As might be expected, the experimental data presented in figure 16 indicate that neutral stability occurs at a higher normal-force coefficient in nitrogen as compared to that obtained in helium and the proper trends are indicated by modified Newtonian theory, if not the actual magnitudes.

CONCLUDING REMARKS

An experimental investigation of the longitudinal stability and performance characteristics of three similar ballistic-type spacecraft configurations has been conducted at a Mach number of 24.5 in helium. An additional brief investigation was made to determine the effectiveness of a small chin flap mounted on a symmetrical blunt-face configuration. The Reynolds number, based on the maximum configuration diameter, was 0.57×10^6 .

A comparison of the results indicated that, based on performance considerations alone, the configuration incorporating a sharp-edge heat shield and a 30° half-angle conical afterbody was the best configuration of the three shapes tested. Furthermore, this shape required the least center-of-gravity displacement to trim at a given lift or lift-drag ratio.

It is probable, however, that other aspects of the reentry problem (principally aerodynamic-heating considerations) would compromise the selection of this shape. Consideration of possible local aerodynamic-heating problems at the edge of the heat shield and over the vehicle afterbody may lead to the choice of an alternative shape employing a corner radius on the heat shield of 5 percent of the maximum vehicle diameter. In addition, it was demonstrated that this configuration was capable of the highest lift-drag ratio of the three shapes tested before exposing the afterbody to the flow.

The control of these blunt axisymmetrical vehicles was considered and it was shown that small center-of-gravity displacements away from the vehicle axis of symmetry would permit the vehicles to be trimmed up to maximum lifts and lift-drag ratios. The chin flap, an alternative means of control, was shown to be most effective at deflection angles below about 100° .

A comparison of data obtained in nitrogen at a Mach number of 18 with similar data obtained at a Mach number of 24.5 from the present tests indicated the degree of simulation which can be expected when using helium to determine the stability and performance of blunt capsule-type configurations. The experimental results obtained in nitrogen and helium generally followed the trends indicated by air- and helium-modified Newtonian theory; however, the increments in drag near zero angle of attack predicted by modified impact theory were generally smaller than those experimentally measured. In addition, the maximum lift-drag ratio in nitrogen was smaller than that measured in helium. Both of these effects may be attributed to the order of magnitude difference in Reynolds numbers of the tests rather than to the effect of the difference in specific-heat ratios of the gases.

Langley Research Center,
National Aeronautics and Space Administration,
Langley Station, Hampton, Va., May 21, 1962.

REFERENCES

1. Faget, Maxime A., Garland, Benjamin J., and Buglia, James J.: Preliminary Studies of Manned Satellites - Wingless Configuration: Nonlifting. NASA TN D-1254, 1962. (Supersedes NACA RM L58EO7a.)
2. Chapman, Dean R.: An Approximate Analytical Method for Studying Entry Into Planetary Atmospheres. NASA TR R-11, 1959. (Supersedes NACA TN 4276.)
3. Eggers, Alfred J., Jr., and Wong, Thomas J.: Re-Entry and Recovery of Near-Earth Satellites, With Particular Attention to a Manned Vehicle. NASA MEMO 10-2-58A, 1958.
4. Wong, Thomas J., Goodwin, Glen, and Slye, Robert E.: Motion and Heating During Atmosphere Reentry of Space Vehicles. NASA TN D-334, 1960.
5. Love, Eugene S., Henderson, Arthur, Jr., and Bertram, Mitchel H.: Some Aspects of Air-Helium Simulation and Hypersonic Approximations. NASA TN D-49, 1959.
6. Ladson, Charles L.: A Comparison of Aerodynamic Data Obtained in Air and Helium in the Langley 11-Inch Hypersonic Tunnel. NASA TM X-666, 1962.
7. Erickson, Wayne D.: Real-Gas Correction Factors for Hypersonic Flow Parameters in Helium. NASA TN D-462, 1960.
8. Armstrong, William O.: Effect of Various Forebody Modifications on the Static Longitudinal Stability and Control Characteristics of a Reentry Capsule at a Mach Number of 9.6. NASA TM X-469, 1961.
9. Henderson, Arthur, Jr.: Recent Investigations of the Aerodynamic Characteristics of General and Specific Lifting and Nonlifting Configurations at Mach 24 in Helium, Including Air-Helium Simulation Studies. Presented at the Specialists' Meeting on the High Temperature Aspects of Hypersonic Flow (Rhode-Saint-Genese, Belgium), AGARD, Apr. 1962.

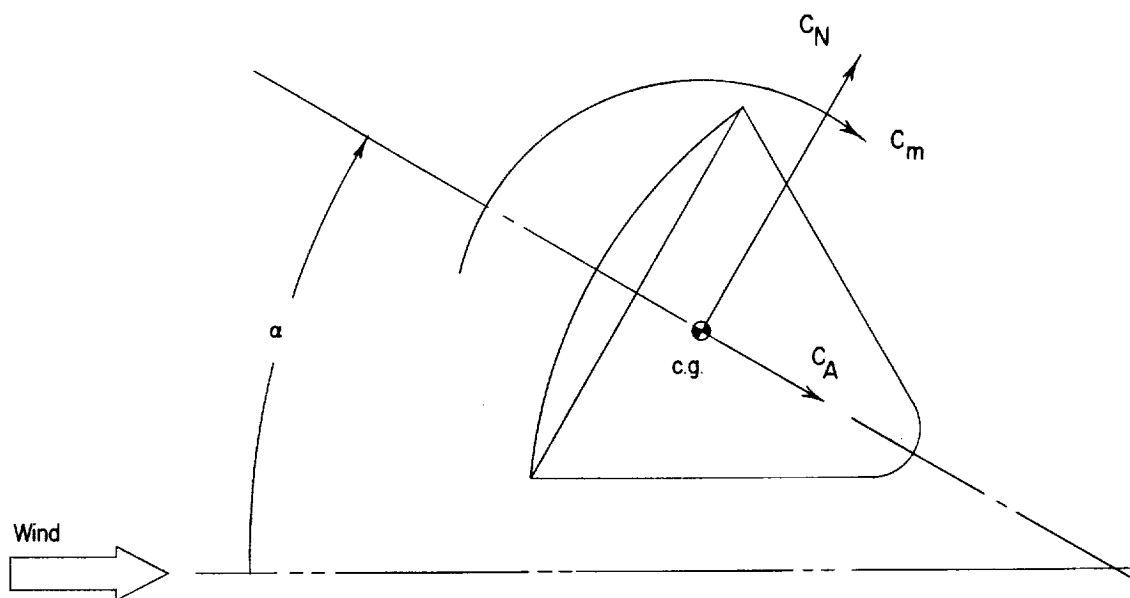


Figure 1.- The body-axis system. Arrows indicate positive directions.

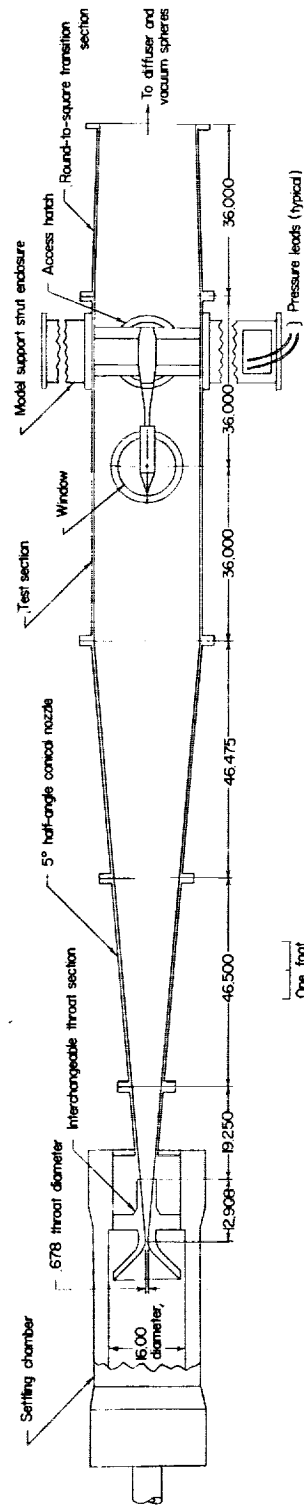


Figure 2.- Schematic diagram of the Langley 22-inch helium tunnel. All dimensions are in inches unless otherwise noted.

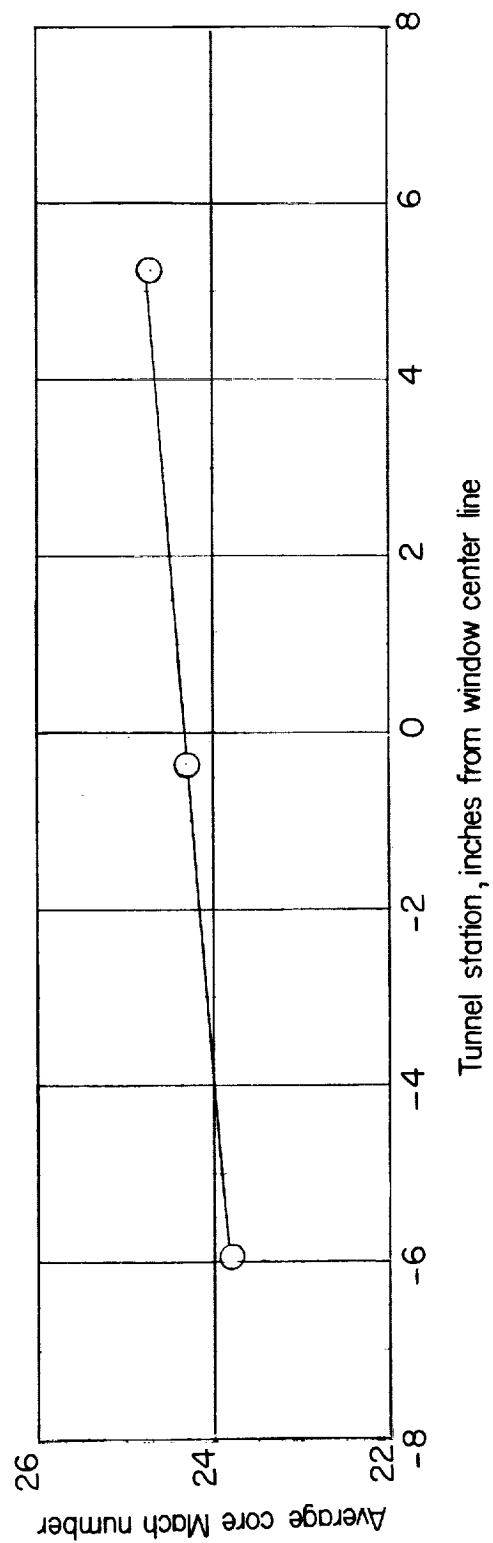
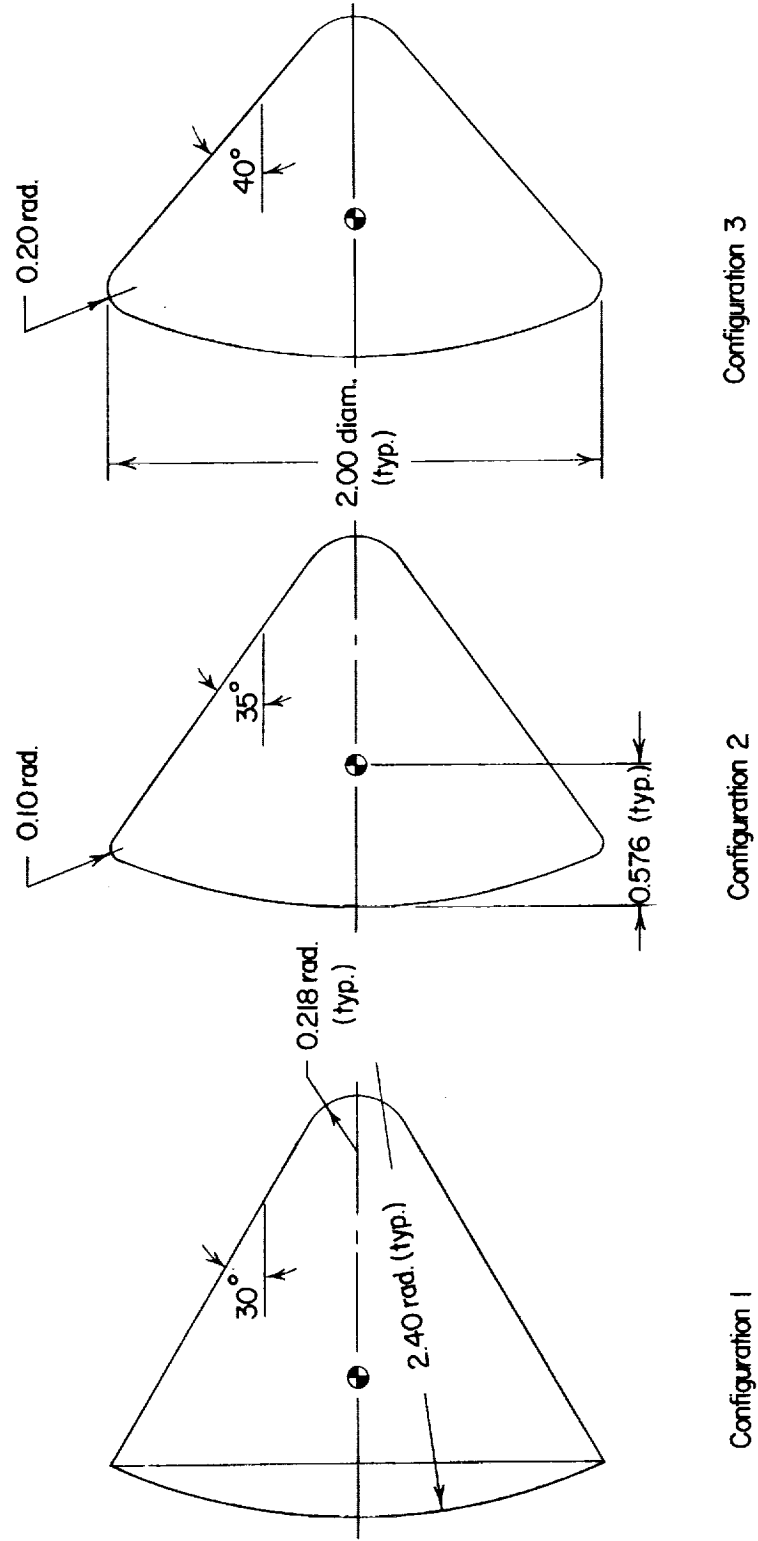


Figure 3.- Test-section Mach number calibration at $p_t = 1,000 \text{ lb/sq in. gage.}$



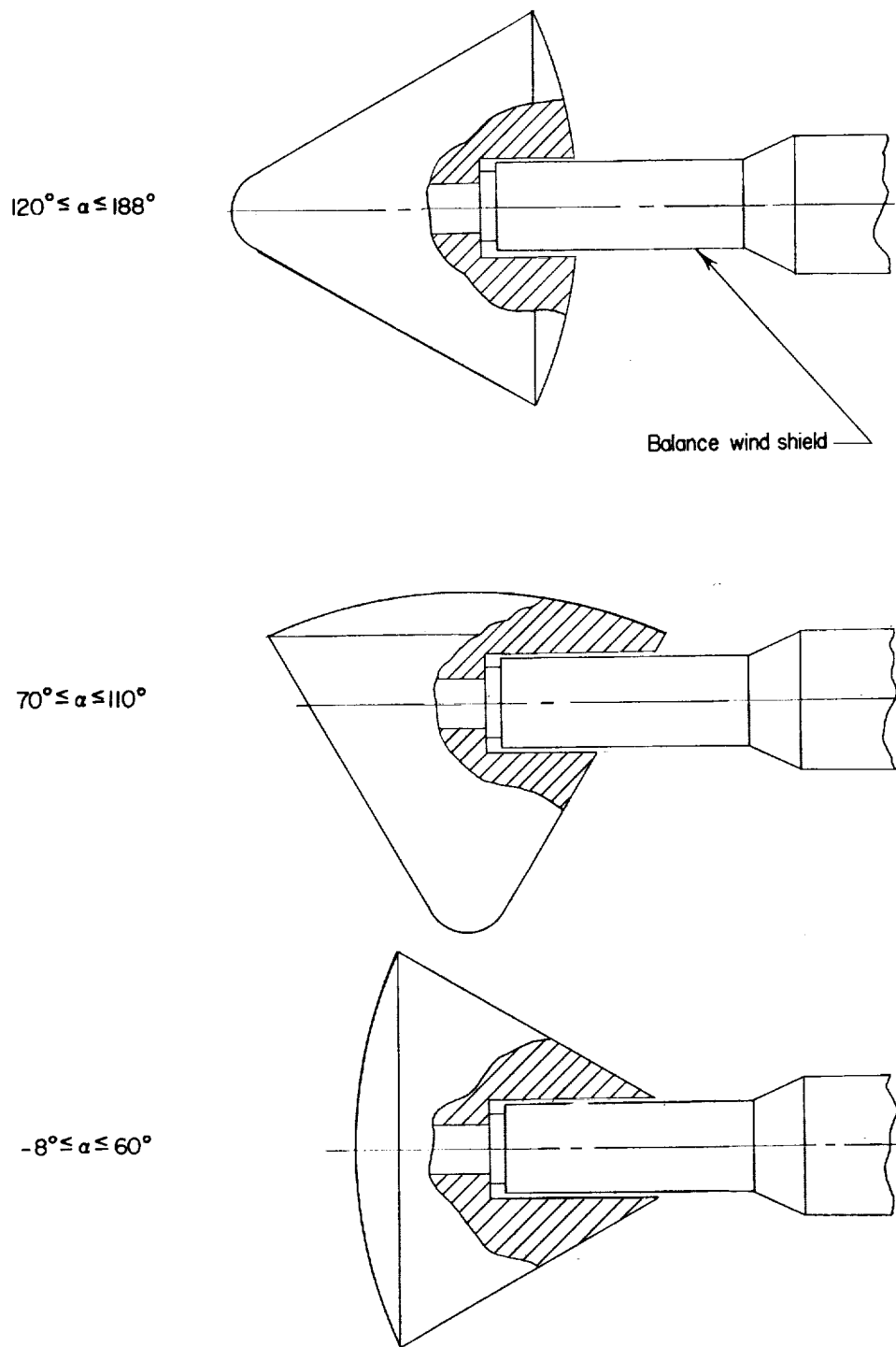


Figure 5.- Typical model-balance arrangements used to obtain $\alpha = -8^\circ$ to 188° .

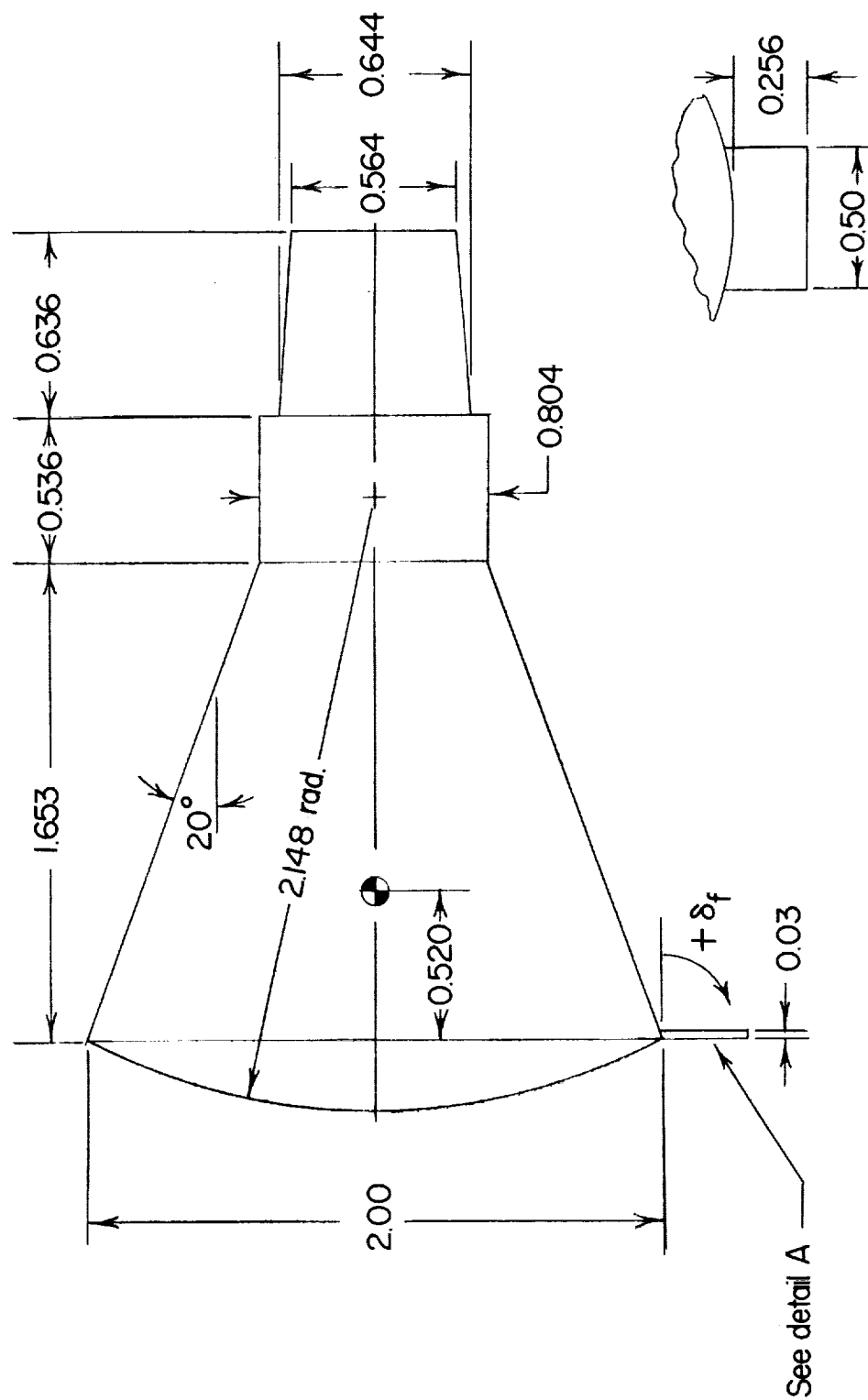
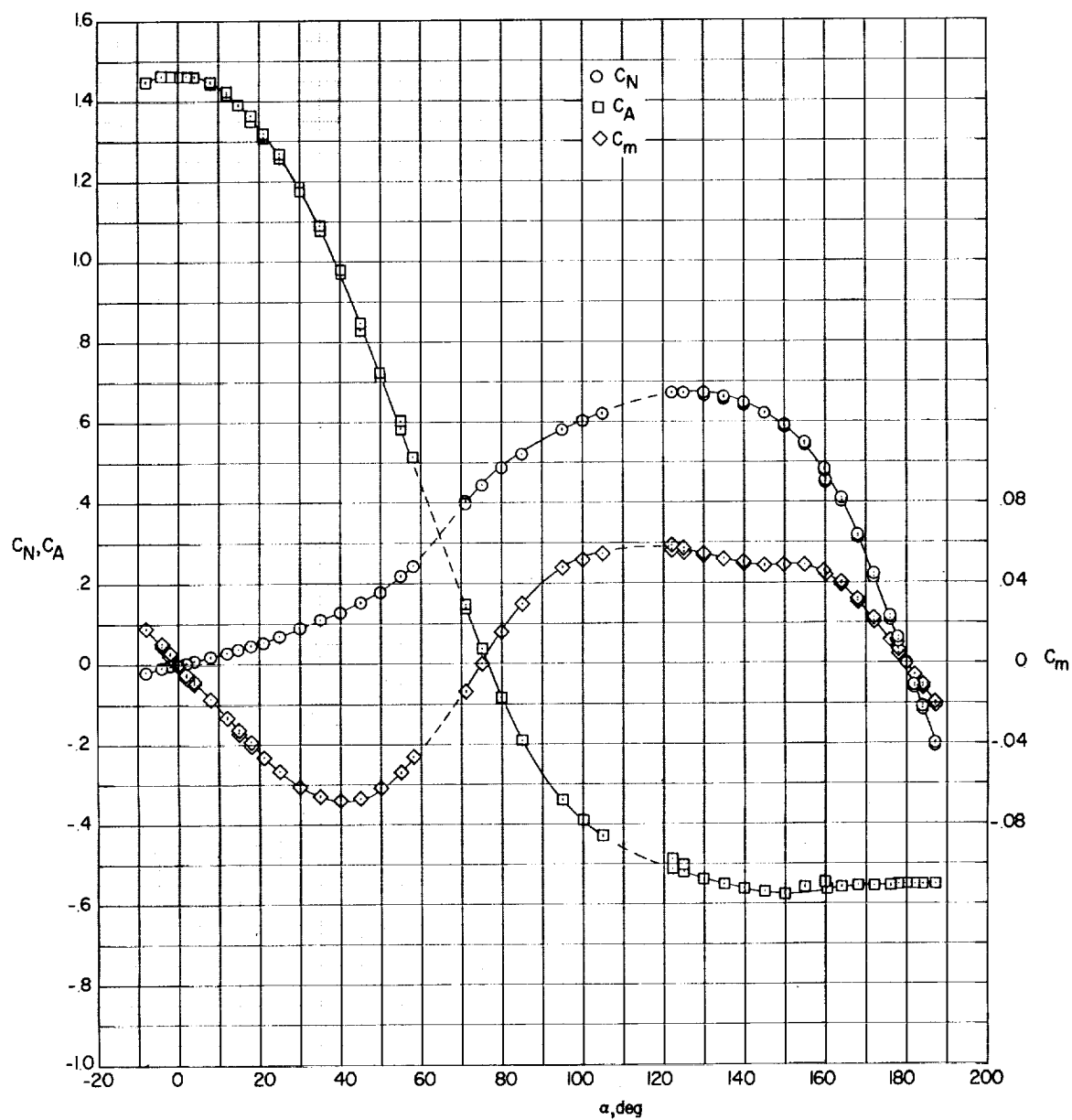
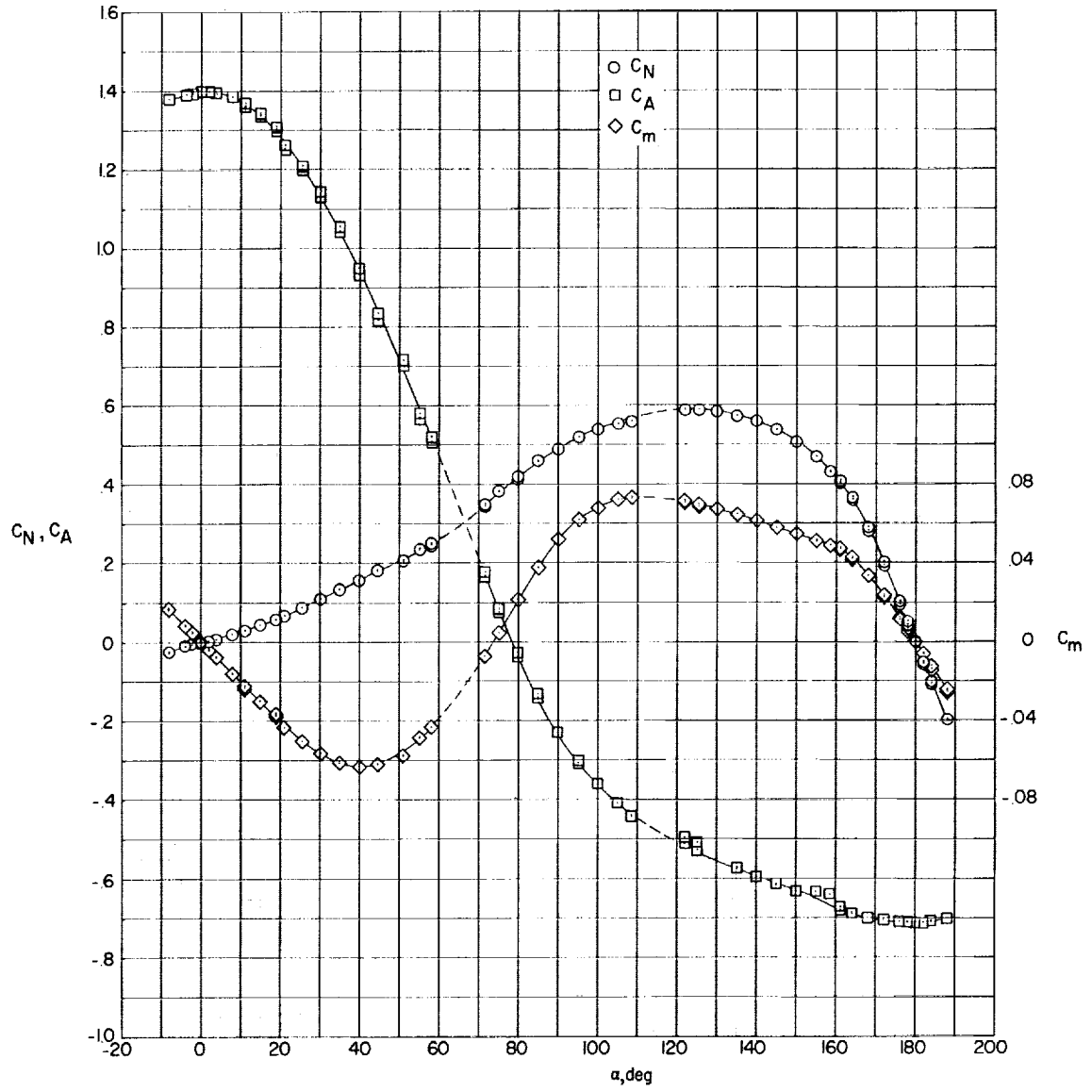


Figure 6.- Dimensions of the model used to determine flap effectiveness. Linear dimensions are in inches.



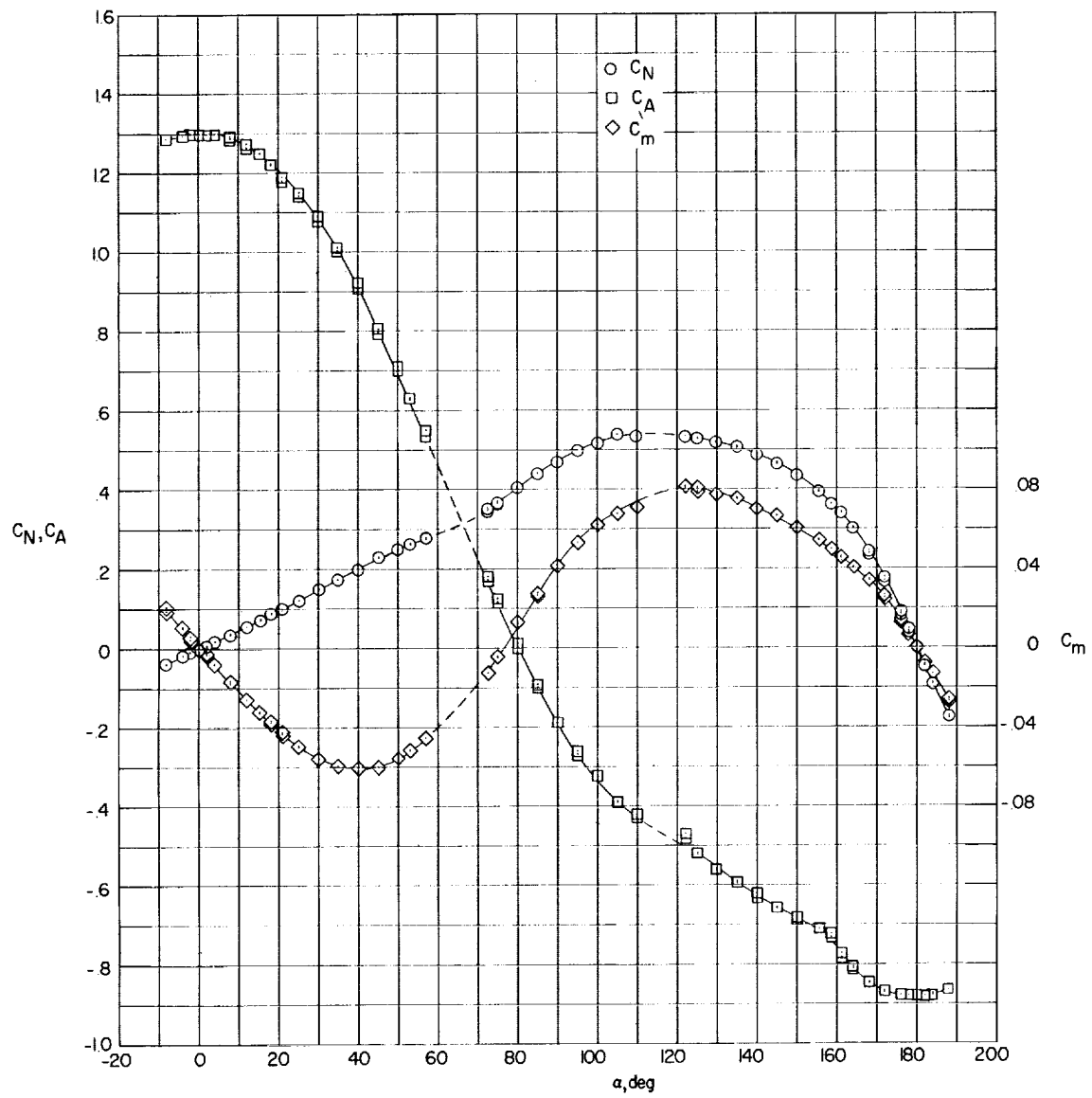
(a) Configuration 1.

Figure 7.- Longitudinal characteristics of the three configurations.



(b) Configuration 2.

Figure 7.- Continued.



(c) Configuration 3.

Figure 7.- Concluded.

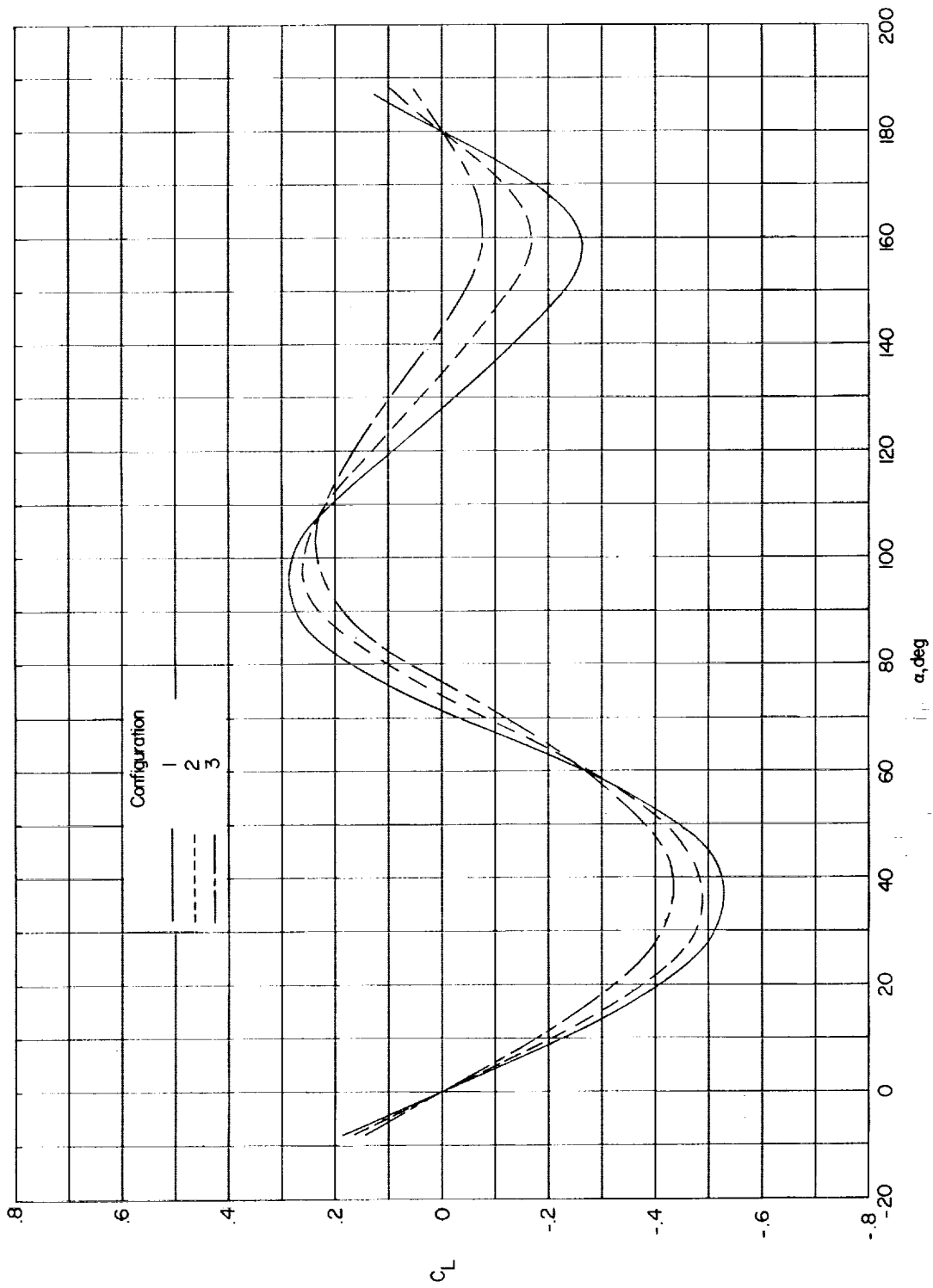


Figure 8.- The variation of lift coefficient with angle of attack for the three configurations.

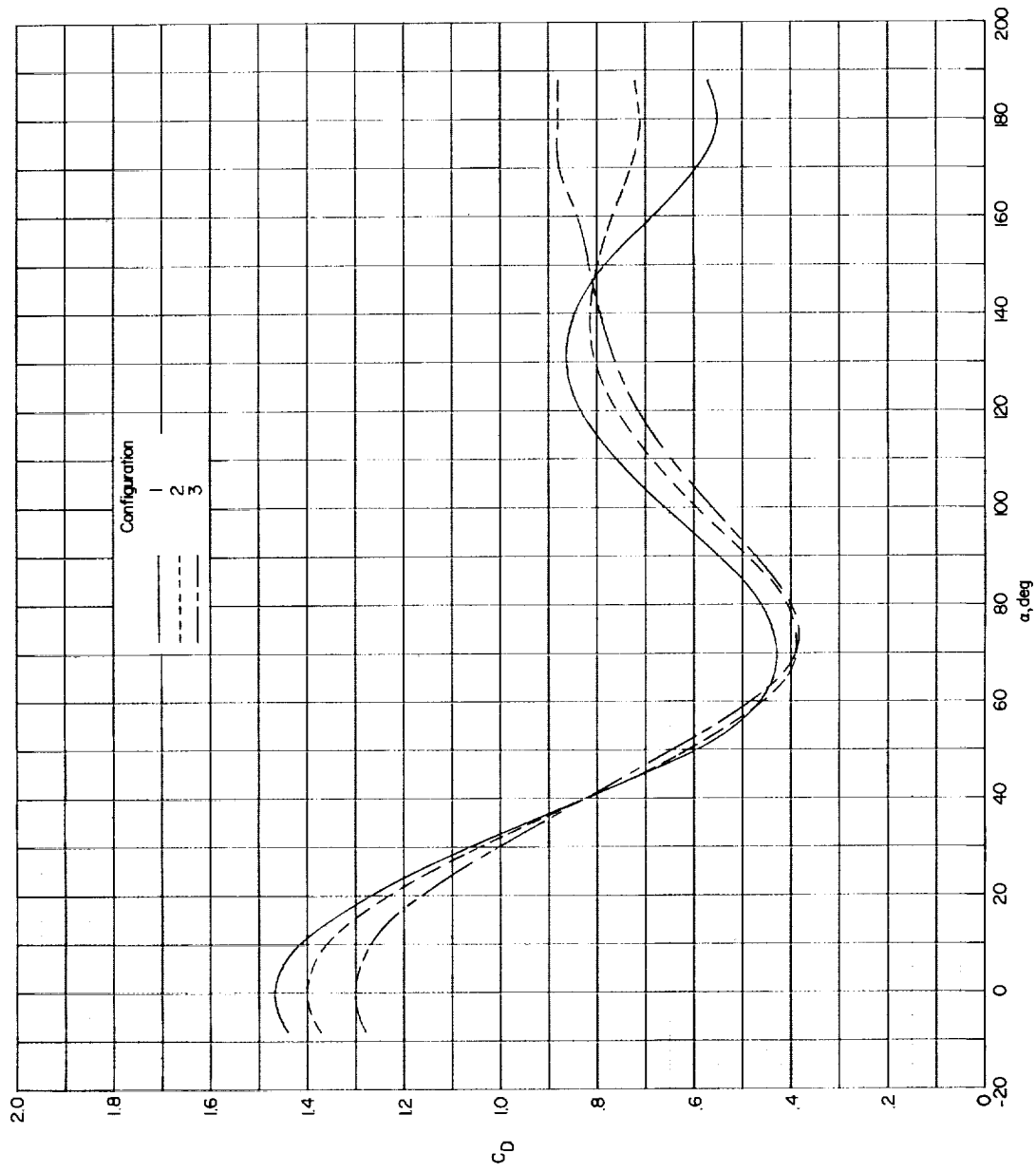


Figure 9.- The variation of drag coefficient with angle of attack for the three configurations.

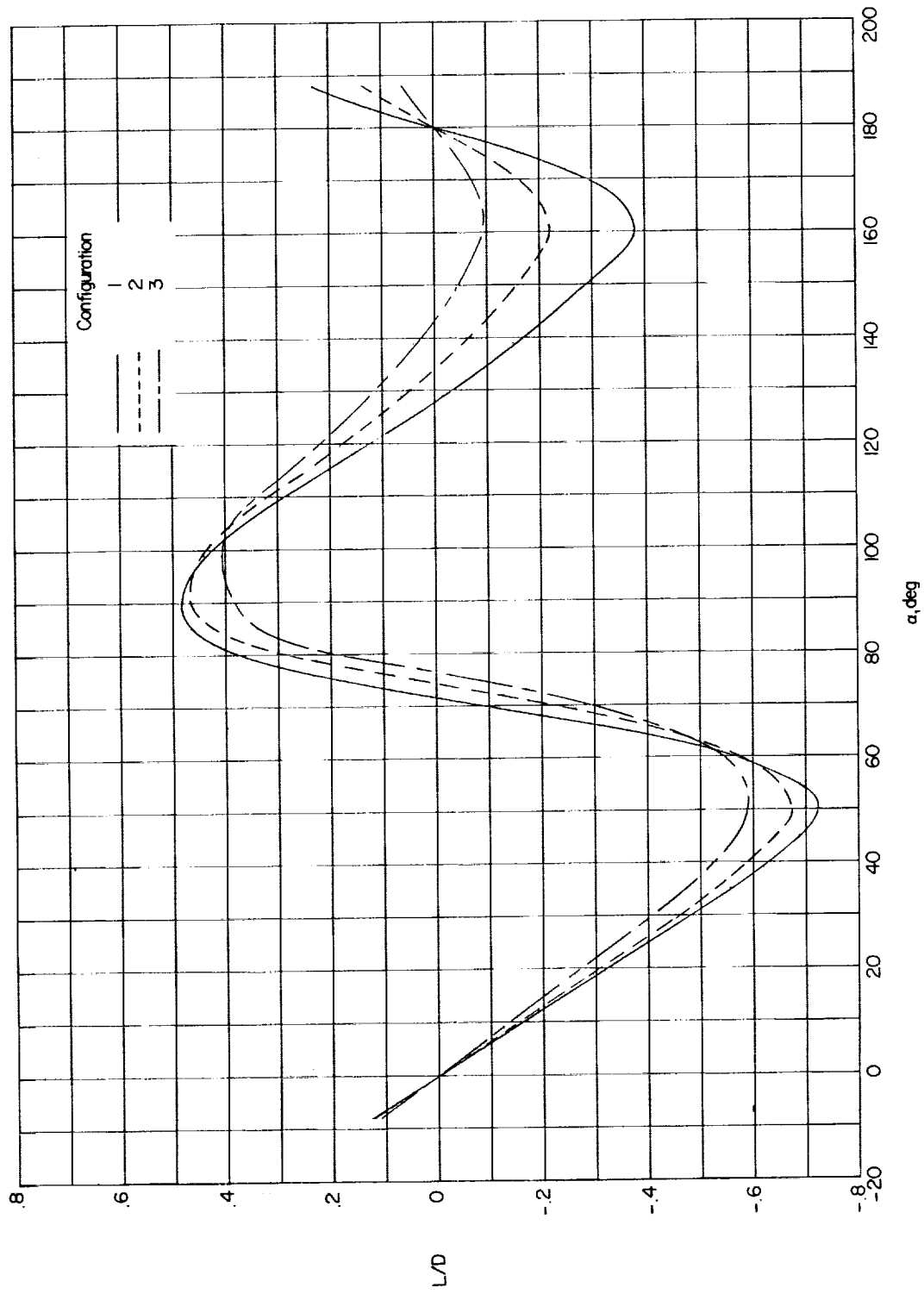


Figure 10.- The variation of lift-drag ratio with angle of attack for the three configurations.

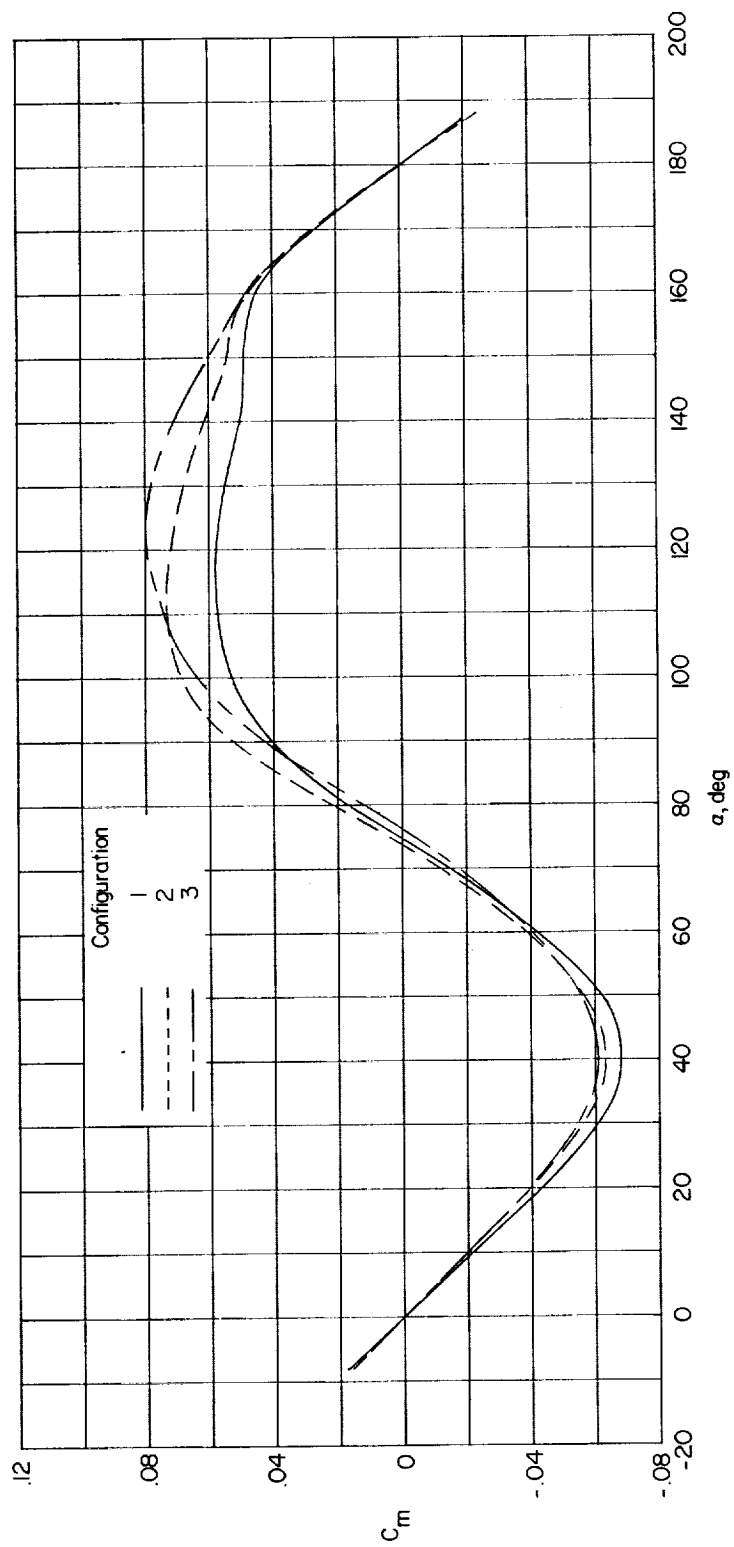


Figure 11.- The variation of pitching-moment coefficient with angle of attack for the three configurations.

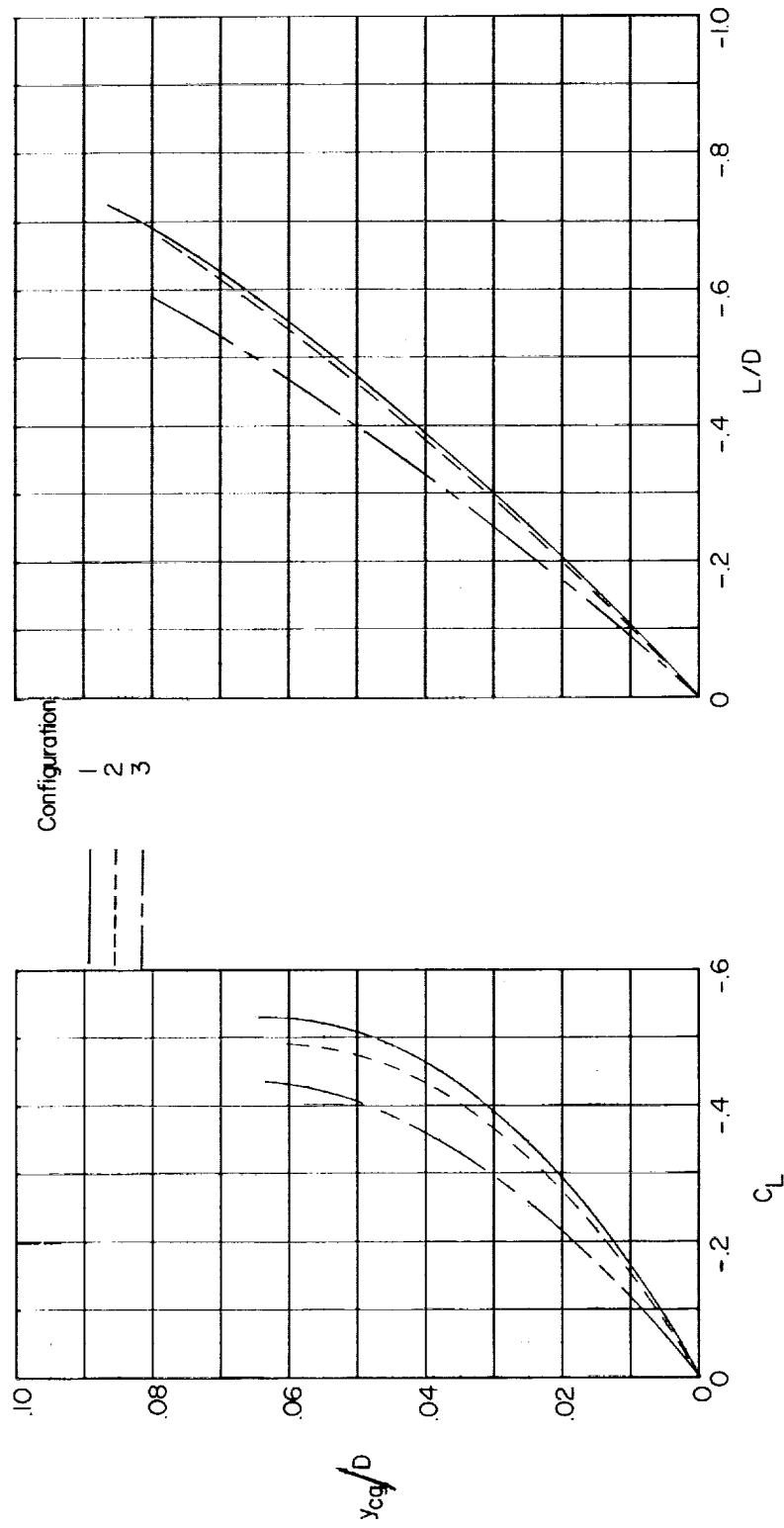
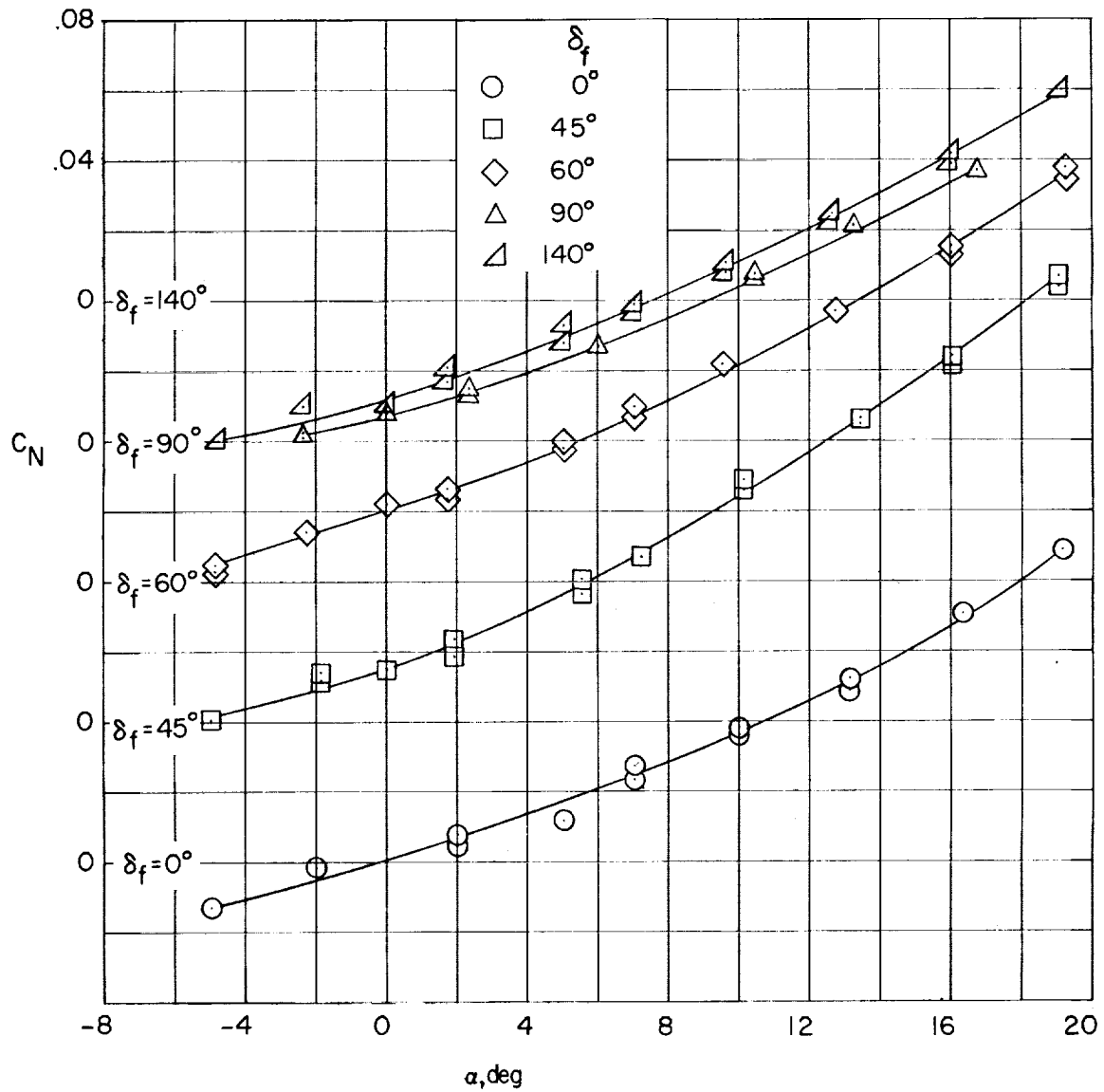
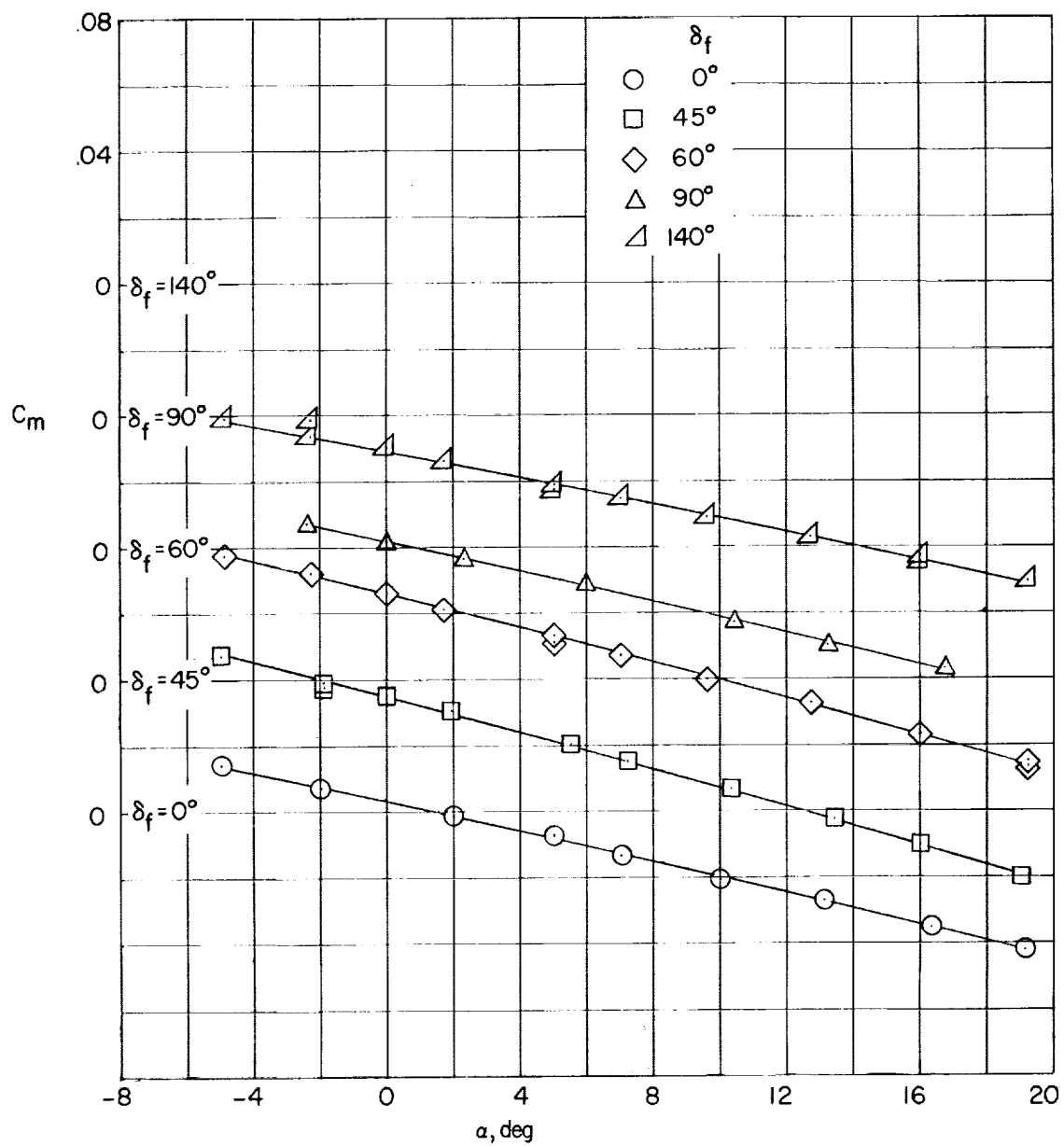


Figure 12.- Vertical center-of-gravity offset required to trim at various lift coefficients and lift-drag ratios. $\frac{x_{cg}}{D} = 0.288$.



(a) Normal-force coefficient.

Figure 13.- Longitudinal characteristics of a ballistic spacecraft configuration equipped with a chin flap. $M = 24.3$; $R = 0.57 \times 10^6$.



(b) Pitching-moment coefficient.

Figure 13.- Concluded.

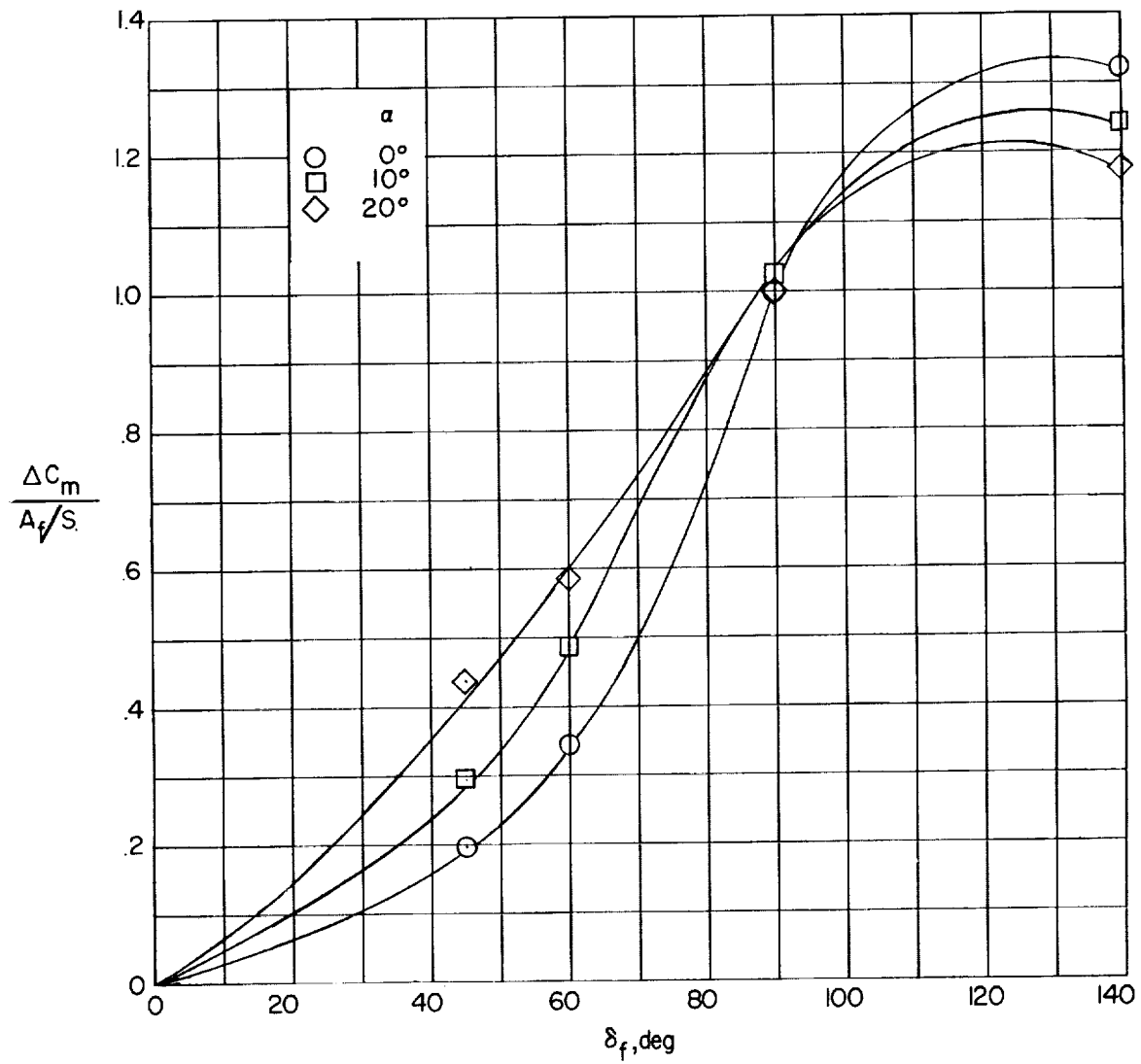


Figure 14.- Effectiveness of a chin flap at hypersonic speeds.

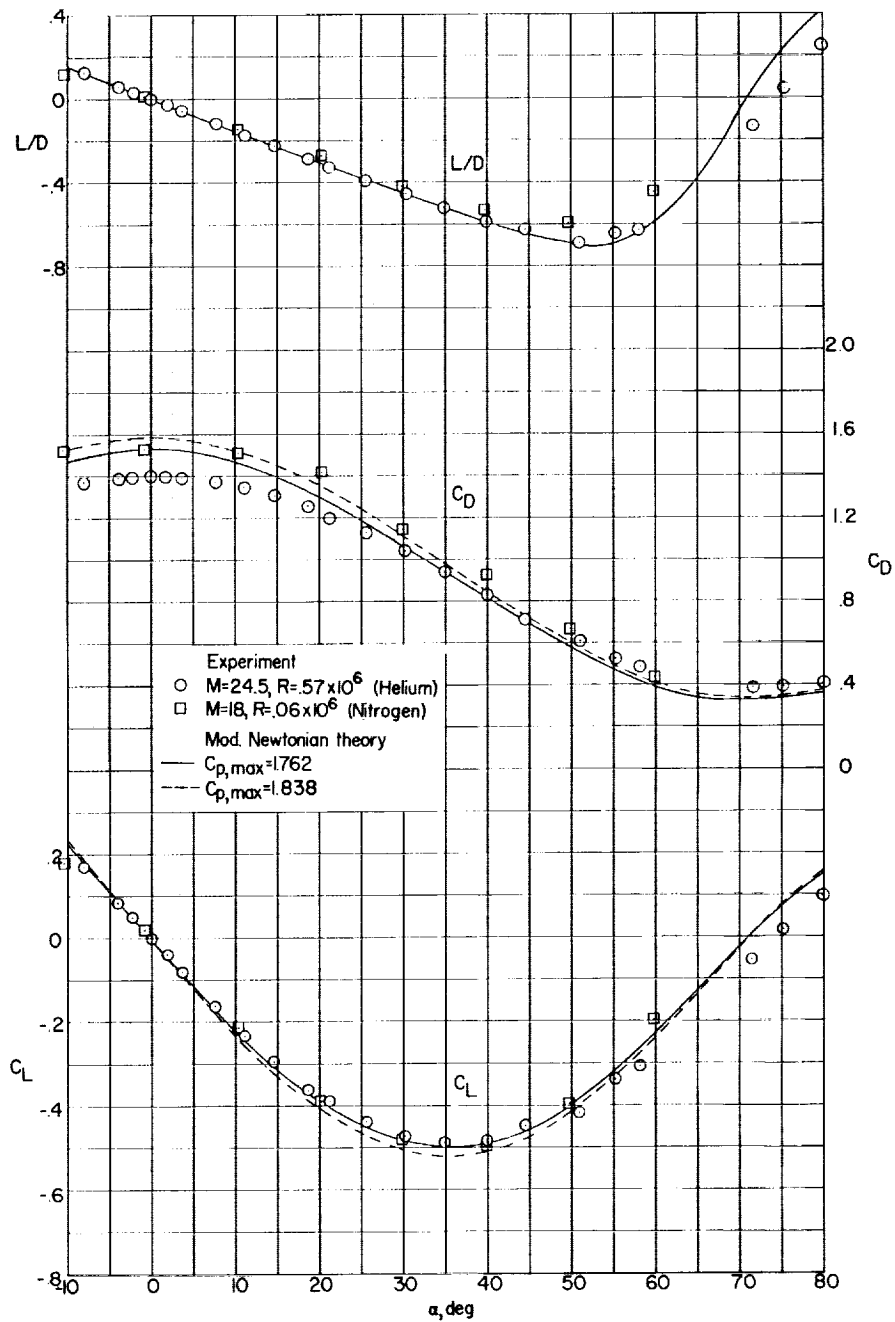
(a) C_L , C_D , and L/D .

Figure 15.- The longitudinal stability and performance characteristics of configuration 2 as determined from experiments in nitrogen and helium and by modified Newtonian theory.

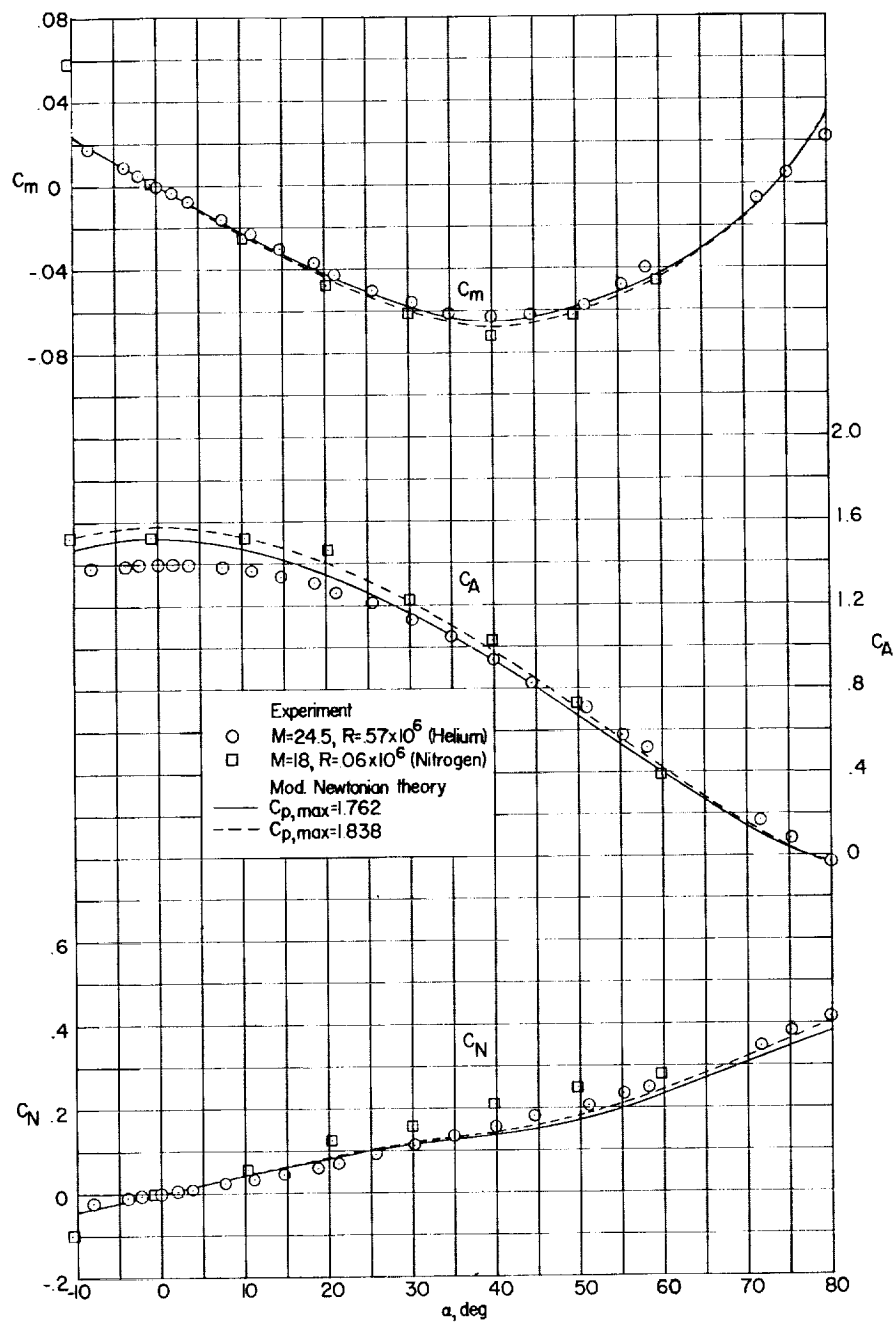
(b) C_N , C_A , and C_m .

Figure 15.- Concluded.

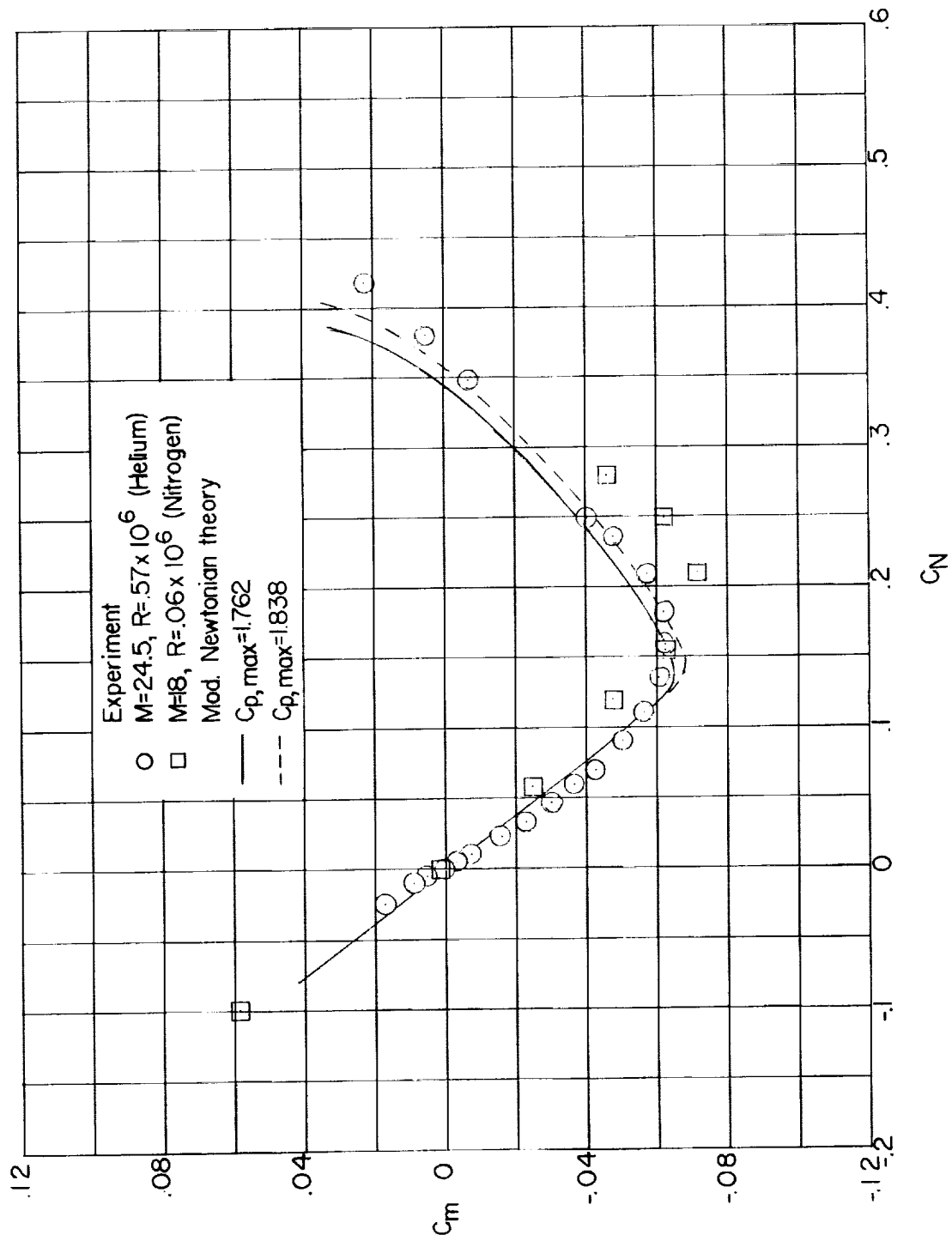


Figure 16.- The longitudinal stability of configuration 2.

<p>NASA TN D-1379 National Aeronautics and Space Administration. STATIC LONGITUDINAL STABILITY AND PERFORMANCE OF SEVERAL BALLISTIC SPACECRAFT CONFIGURATIONS IN HELIUM AT A MACH NUMBER OF 24.5. Patrick J. Johnston and Curtis D. Snyder. August 1962. 36p. OTS price, \$1.00. (NASA TECHNICAL NOTE D-1379)</p> <p>The angle-of-attack range was from -80 to 188°, and the Reynolds number, based on the maximum configuration diameter, was approximately 0.57×10^6. A comparison of the results showed that the configuration having a 35° half-angle conical afterbody with a heat-shield corner radius of 5 percent of the maximum diameter developed the highest lift-drag ratio without exposing the afterbody to the flow. An additional comparison of data for this configuration obtained by using nitrogen and helium test media indicated the degree of simulation which may be expected on blunt shapes tested in helium.</p>	<p>I. Johnston, Patrick J. II. Snyder, Curtis D. III. NASA TN D-1379</p> <p>(Initial NASA distribution: 2, Aerodynamics, missiles and space vehicles; 47, Satellites; 48, Space vehicles; 50, Stability and control.)</p>	<p>I. Johnston, Patrick J. II. Snyder, Curtis D. III. NASA TN D-1379</p> <p>(Initial NASA distribution: 2, Aerodynamics, missiles and space vehicles; 47, Satellites; 48, Space vehicles; 50, Stability and control.)</p>	<p>NASA TN D-1379 National Aeronautics and Space Administration. STATIC LONGITUDINAL STABILITY AND PERFORMANCE OF SEVERAL BALLISTIC SPACECRAFT CONFIGURATIONS IN HELIUM AT A MACH NUMBER OF 24.5. Patrick J. Johnston and Curtis D. Snyder. August 1962. 36p. OTS price, \$1.00. (NASA TECHNICAL NOTE D-1379)</p> <p>The angle-of-attack range was from -80 to 188°, and the Reynolds number, based on the maximum configuration diameter, was approximately 0.57×10^6. A comparison of the results showed that the configuration having a 35° half-angle conical afterbody with a heat-shield corner radius of 5 percent of the maximum diameter developed the highest lift-drag ratio without exposing the afterbody to the flow. An additional comparison of data for this configuration obtained by using nitrogen and helium test media indicated the degree of simulation which may be expected on blunt shapes tested in helium.</p>	<p>I. Johnston, Patrick J. II. Snyder, Curtis D. III. NASA TN D-1379</p> <p>(Initial NASA distribution: 2, Aerodynamics, missiles and space vehicles; 47, Satellites; 48, Space vehicles; 50, Stability and control.)</p>	<p>NASA TN D-1379 National Aeronautics and Space Administration. STATIC LONGITUDINAL STABILITY AND PERFORMANCE OF SEVERAL BALLISTIC SPACECRAFT CONFIGURATIONS IN HELIUM AT A MACH NUMBER OF 24.5. Patrick J. Johnston and Curtis D. Snyder. August 1962. 36p. OTS price, \$1.00. (NASA TECHNICAL NOTE D-1379)</p> <p>The angle-of-attack range was from -80 to 188°, and the Reynolds number, based on the maximum configuration diameter, was approximately 0.57×10^6. A comparison of the results showed that the configuration having a 35° half-angle conical afterbody with a heat-shield corner radius of 5 percent of the maximum diameter developed the highest lift-drag ratio without exposing the afterbody to the flow. An additional comparison of data for this configuration obtained by using nitrogen and helium test media indicated the degree of simulation which may be expected on blunt shapes tested in helium.</p>	<p>I. Johnston, Patrick J. II. Snyder, Curtis D. III. NASA TN D-1379</p> <p>(Initial NASA distribution: 2, Aerodynamics, missiles and space vehicles; 47, Satellites; 48, Space vehicles; 50, Stability and control.)</p>
---	---	---	---	---	---	---

